Coercivity and Phase Transitions of Clustered $Nd_{90-x}Fe_xAl_{10}$ Bulk Hard Magnets

Horia Chiriac and Nicoleta Lupu

National Institute of Research and Development for Technical Physics, 47 Mangeron Blvd., Iasi 6600, Romania

Rapidly and slowly quenched $Nd_{90-x}Fe_xAl_{10}$ glassy alloys with thicknesses up to 3 mm were investigated comparatively by structural and magnetic measurements in the temperature range 5–800 K and external fields up to 9 T. The glass-forming ability decreases increasing Fe content. Room temperature coercivities of over 0.6 T are observed, depending on composition and external field. The huge increase of the coercive field up to 5.5 T at low temperatures as well as the dependence on the cooling rate are supposed to result from the non-collinear magnetic structures developed in these amorphous alloys. From DC and AC magnetic measurements combined with neutron diffraction results we conclude that the structure, which is quenching conditions dependent, consists of a packing of nanometer-sized clusters. The topological and magnetic structures of $Nd_{90-x}Fe_xAl_{10}$ melt-spun ribbons and cast rods in a wide range of temperatures and for different x values are modelled using the reverse Monte Carlo method (RMC). The hypotheses of a cluster model, in which exchange interactions, local random anisotropies and thermal effects are competing, are proposed.

1. Introduction

Although the mechanisms that determine the specific magnetic behaviour of metallic glasses were studied in detail in the past, there are still many aspects unclear especially about the intrinsic mechanisms determining the magnetic properties of rare earth-transition metal amorphous alloys. The magnetic structures in these alloys will be strongly influenced by the local anisotropy field at the rare earth sites, just as in crystalline similar compounds. If the magnitude of the random anisotropy is large compared to the exchange, the local anisotropy fields orients the spins along their anisotropy axes. Random orientation of anisotropy axes gives way to a magnetically disordered state. To transform the system in a ferromagnetic one it is enough just to put it in a sufficiently strong magnetic field. After the field removal all spins will be directed in a hemisphere.[1] If the anisotropy is weak enough, exchange favours long-range ferromagnetic order.

The magnetism of light rare earth-Fe alloys produced by rapid quenching from the melt has been a great stimulus for research, especially since the discovery of the high coercive fields over 10 kOe at room temperature in melt-spun Nd–Fe and Pr–Fe amorphous alloys.[2,3] There were many attempts to explain the coercivity mechanism in Nd–Fe and Pr–Fe amorphous alloys, which were not necessarily consistent with each other. One of the proposed and most accepted ideas was the existence of a new metastable amorphous or nanocrystalline phase, so called A_1 phase that can not be synthesized in normal conditions.[4]

Recently, similar magnetic behaviour was reported for Nd–TM-based (TM=Fe, Co) ternary amorphous alloys with additions of Al and Si. Moreover, these alloys can be cast in bulk shapes with dimensions of millimetres due to their large glass forming ability and exhibit large coercivities in the as-quenched state.[5–10] Although X-ray diffraction studies emphasized fully amorphous structures for the most of the investigated Nd–Fe–(Al, Si) melt-spun ribbons and cast samples,

the strong dependence of the coercive field on the quenching conditions and temperature as well as the weak ferromagnetic behaviour observed after crystallization suggested that the amorphous structure is not homogenous consisting in at least two distinct short-range chemical ordered regions.[11–15] Apparently, the results are in contradiction to the conventional understanding of the relationship between coercivity mechanisms and microstructure. The large coercivities are not characteristics to the amorphous structure because this structure is considered to be isotropic and the increase of coercivity arises from the impediments to domain wall-motion, such as grain boundaries, defects, pinning centres, *etc.*[16]

In the following we try to clarify the relationship between the microstructure and magnetic characteristics and to better understand the origin of coercivity in $Nd_{90-x}Fe_xAl_{10}$ ($x = 20$–60 at%) amorphous melt-spun ribbons and cast rods with a variety of different techniques to characterize the material in a wide range of temperatures (4–800 K) and comparing the results with the simulated structures under the hypothesis of a random atomic configuration.

2. Experimental Procedure

The quenched alloys were prepared by first arc melting commercially available components: Nd (99.9%), Fe (99.97%), Al (99.9%), in Cu crucibles and then melt-spinning and suction casting under an atmosphere of Ar. The measured samples were $Nd_{90-x}Fe_xAl_{10}$ melt-spun ribbons ($x = 20$–60) with thicknesses between 25 and 120 μm and width of 2–4 mm and cast rods ($x = 35$–50) with diameters up to 2 mm prepared by suction casting. In the following we presume, in agreement with other authors, the melt-spun ribbons as bulk samples for two reasons: the preparation technique is a continuous method and the dimensions of the ribbons, including thickness, are higher than the dimensions of the amorphous thin films. Different thicknesses for melt-spun ribbons were obtained by changing the surface wheel velocity from 25 to

$5\,ms^{-1}$, and maintaining the other parameters at well established values. Rods with diameters between 0.5 and 2 mm were prepared by copper mould suction casting method in an Ar atmosphere. The master alloy was melted in a water cooled copper mould in arc melting chamber and suction after that in another cooled mould with different internal diameters by applying a sucking pressure (about 1 at) at the bottom part of this mould. X-ray diffraction (XRD) investigations performed on both sides of the ribbons and on powders obtained by milling the thick ribbons and cast rods confirmed that most of the samples were nominally amorphous.

Because of the low penetration depth of X-rays (few nanometers) in Nd–Fe-based alloys,[17] and due to the limited amount of sample that can be investigated by XRD as well as to the controversial amorphous microstructure supposed to exist in Nd–Fe-based amorphous alloys, neutron diffraction measurements were carried out using the Studsvik Liquids and Amorphous Materials Diffractometer (SLAD) at the R2 reactor, Studsvik Neutron Research Laboratory, Sweden. The melt-spun ribbons, about 3–4 g each, were packed tightly and sealed inside a standard vanadium container, whereas the cast rods 4 cm long were stuck together to fill out the container. The sample data were corrected for background and container scattering, container absorption and sample self-absorption, multiple and inelastic scattering, and normalized to an absolute scale.[18] Data were collected between 15 and 800 K. The reduced radial distribution functions, $G(r)$, were obtained from the measured total structure factor, $S(Q)$, by using MCGR,[19] a program available on SLAD that uses Monte Carlo method to "generate" possible $G(r)$, and then modifies these to fit the measured data, $S(Q)$. But the main problem in the analysis of the diffraction data on disordered systems is the lack of any general method to produce structural models that agree quantitatively with the data. The reverse Monte Carlo (RMC) method overcomes this problem.[20] In the RMC simulations reported here, systems containing 2000–2500 particles were used. The input experimental data was $S(Q)$. The experimental number density, ρ, was $0.0055\,nm^{-3}$. Closest-approach distances were determined on the basis of the corresponding experimental data. All calculations were started from hard spheres random configurations. To reach the equilibrium (the closest fit to the experiment), 6.5–8.5×10^6 accepted moves had to be completed.

DC-magnetic measurements at room temperature and above, but not exceeding 1100 K, in applied fields limited to $640\,kAm^{-1}$, were carried out using a homemade vibrating sample magnetometer (VSM). The variations of the magnetization and coercive field at low temperatures were investigated using a SQUID MPMS$_2$ magnetometer (maximum field $800\,kAm^{-1}$) and an Oxford MagLab VSM (maximum field $7.2\,MAm^{-1}$). AC-susceptibility in the temperature range 4.2–300 K was measured by using a very sensitive susceptometer in AC magnetic fields between 160 and $1600\,Am^{-1}$ and frequencies ranging from 29.1 to 291 Hz. The magnetic field was applied in the axial direction of the samples.

Magnetic measurements offered information about intrinsic and extrinsic magnetic properties taking in consideration the response of either disordered and ordered regions in the material, so they are strongly influenced by the structural environments of the atoms. Mössbauer spectroscopy,

considered a complementary method for diffraction techniques, offers information both about the atomic scale environments and about the relaxation and dynamic phenomena that take place in materials. Despite of these the major problem in studying Mössbauer spectra of amorphous materials is the fitting procedure. Mössbauer spectra measured for $Nd_{90-x}Fe_xAl_{10}$ ($x = 40$ and 50) melt-spun ribbons at room temperature were fitted by using the distribution of hyperfine fields linearly correlated to that of the isomer shift, and the quadrupole component if any.

3. Results

3.1 Neutron Diffraction Results

Figure 1 presents the room temperature neutron diffraction patterns for $Nd_{50}Fe_{40}Al_{10}$ melt-spun ribbons with thicknesses of 25 and 120 μm as well as for a cast rod 1 mm in diameter. The split first peak and the pronounced structure at higher angles are features not present in the patterns for the other amorphous alloys with dense random packed atomic structures but they were observed in Nd–Fe binary amorphous alloys.[21] The split is more pronounced for the thicker ribbon than for the thin ones and the cast rods. We suppose this behavior being
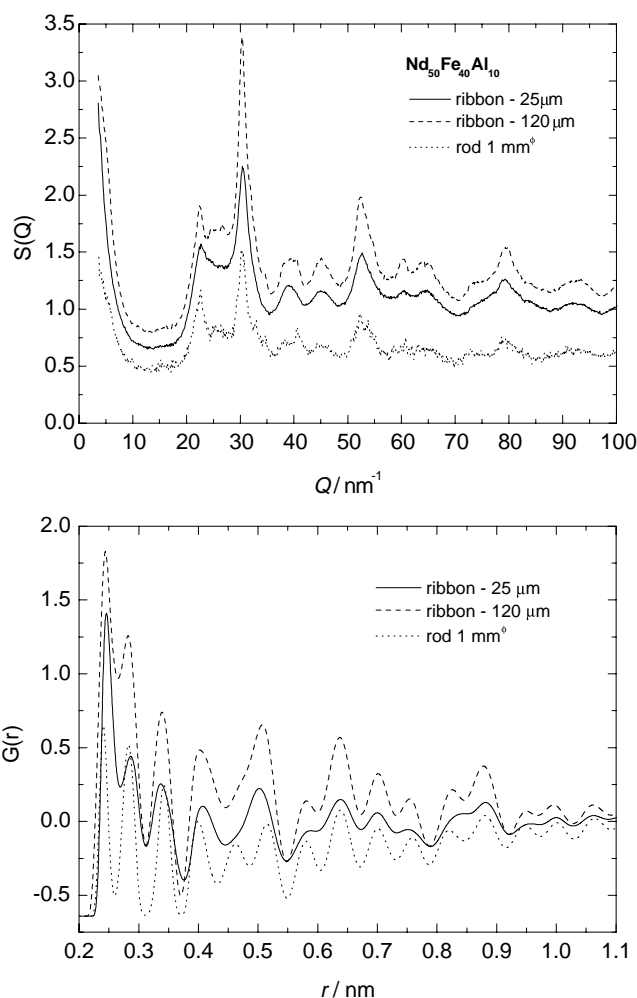

Fig. 1 Neutron diffraction patterns as a function of wave-vector, $Q = 4\pi \sin\theta/\lambda$, and reduced radial distribution function, $G(r) = 4\pi r^2 \rho(r)$, for $Nd_{50}Fe_{40}Al_{10}$ bulk amorphous alloys.

related to the more heterogeneous disordered structure developed in the thick ribbons due to the intermediary values of the cooling rate of 10^3–10^4 Ks^{-1} in comparison with 10^5–10^6 Ks^{-1} for thin melt-spun ribbons and 10^1–10^2 Ks^{-1} for the cast rods. The reduced radial distribution functions, $G(r)$, obtained by Fourier transformation of the total structure factor, $S(Q)$, show first neighbors peaks at 0.254, 0.285, 0.336 and 0.420 nm. The peak at 0.254 nm is at the position expected for the nearest neighbor Fe atoms in the dense random packing (DRP) model; the other peaks cannot be correlated to combinations of the radii of Nd (0.182 nm), Al (0.143 nm) or Fe (0.127 nm) atoms as predicted by the DRP model. This disagreement, which is particular to the case of the present light rare earth-Fe alloys, could be ascribed to the development of a new type of disordered structure, in which few Fe atoms form clusters randomly distributed, while Nd and Al are distributed randomly between these clusters. The decrease of the Fe content below 40 at% does not change very much the structure factor, $S(Q)$, regarding the samples thickness, whereas the increase of the Fe content above 40 at% results in the decrease of the glass-forming ability and the precipitation of crystalline phases, as it is shown in Fig. 2. These results agree very well with XRD and DSC previously reported results.[22]

The decrease of the temperature below room temperature does not change significantly the structure factor, $S(Q)$, as shown in Fig. 3(a), whereas the increase of the temperature above the crystallization temperature ($T_x \cong 440°C$) leads to the samples crystallization (Fig. 3(b)). All the samples exhibit the same behaviour.

The results of the reverse Monte Carlo (RMC) atomic configuration modelling for $Nd_{50}Fe_{40}Al_{10}$ amorphous ribbons 25 (a) and 120 μm (b) are presented in Fig. 4. The modelled configurations obtained for partially vitrified $Nd_{30}Fe_{60}Al_{10}$ 25 μm (c) and $Nd_{40}Fe_{50}Al_{10}$ 120 μm (d), respectively, are presented for comparison. Small Fe-based clusters embedded in a homogeneous Nd-based matrix are observed in $Nd_{50}Fe_{40}Al_{10}$ amorphous ribbons, while in the partially vitrified ribbons, regarding the Fe content and thickness, slabs containing Fe and Al and between them isotropically distributed Nd and Fe atoms were found out.

3.2 Magnetic measurements

Neutron diffraction investigations on $Nd_{90-x}Fe_xAl_{10}$ amorphous melt-spun ribbons and cast rods revealed a new type of disordered structure consisting in a dense random packing of nanometer-sized atomic clusters, whose size is dependent on the samples thickness, *i.e.* the preparation conditions. Consequently, one expects complex magnetic behavior dependent on the thickness and the composition. Magnetization and co-
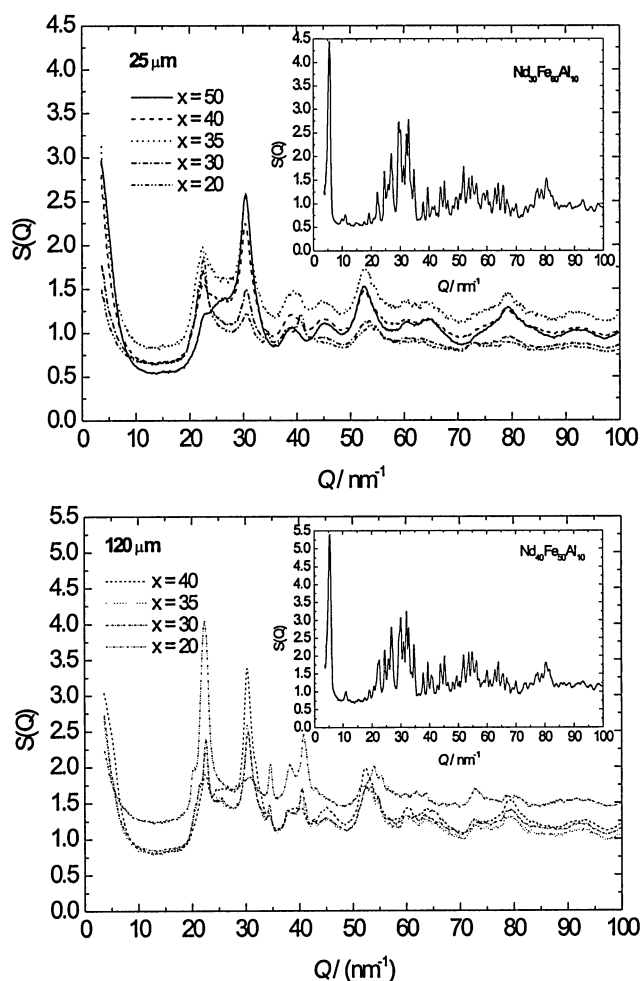

Fig. 2 Structure factor, $S(Q)$, as a function of Fe content for $Nd_{90-x}Fe_xAl_{10}$ melt-spun ribbons with thicknesses of 25 and 120 μm, respectively.
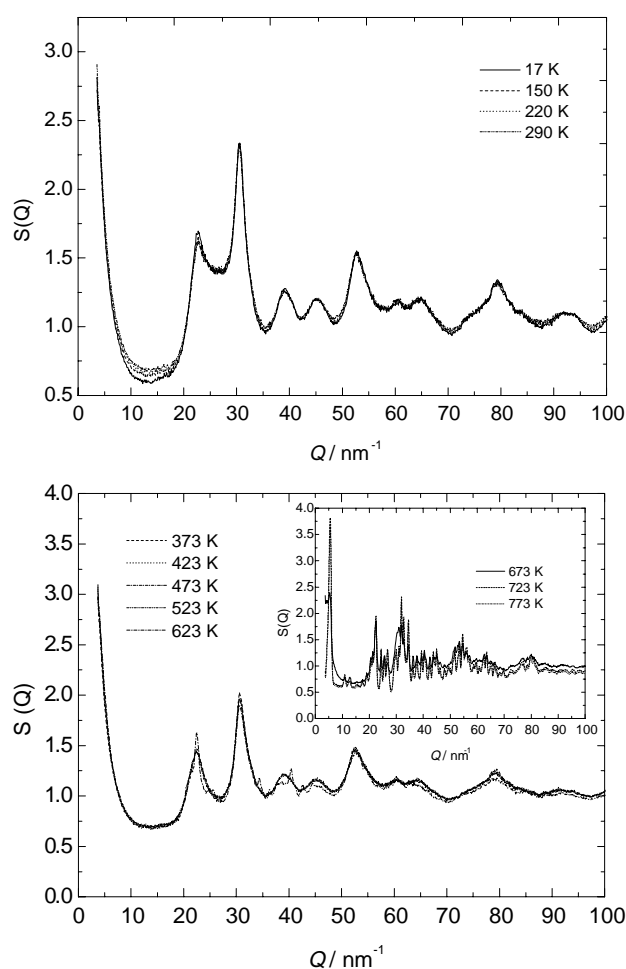
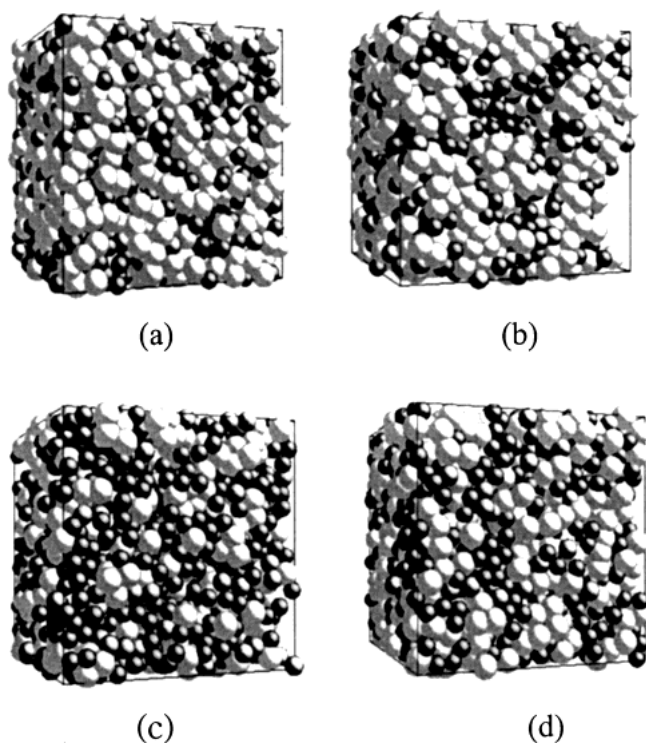Fig. 3 Structure factor, $S(Q)$, as a function of temperature for $Nd_{50}Fe_{40}Al_{10}$ amorphous ribbon 25 μm thickness.

Fig. 4 Reverse Monte Carlo (RMC) modeled atomic structures for $Nd_{90-x}Fe_xAl_{10}$ amorphous ((a) and (b)) and partially vitrified ((c) and (d)) ribbons having 25 μm ((a) and (c)) and respectively 120 μm ((b) and (d)) in thickness (Nd is represented by light gray spheres, Fe by black and Al by dark grey spheres).

Fig. 5 (a) Spontaneous (open symbols) and saturation (at $6.4\,MAm^{-1}$) (full symbols) magnetization of amorphous and partially vitrified $Nd_{90-x}Fe_xAl_{10}$ alloys at room temperature; (b) Coercive field vs. x at room temperature.

ercive field measurements of ribbons and cast rods were performed as a function of the Fe content, thickness, temperature and field.

Figure 5(a) shows magnetization at $6.4\,MAm^{-1}$ and spontaneous magnetization as a function of the Fe content for 3 different kinds of the samples: melt-spun ribbons of 25 and 120 μm and cast rods 1 mm in diameter. The spontaneous magnetizations were obtained by extrapolating the high field data linearly to zero. The corresponding coercive fields at room temperature are presented in Fig. 5(b). The increase of the Fe content results in a continuous increase of the magnetization, regarding the sample type or the structure. The spontaneous magnetization increases with x for the amorphous samples, but decreases drastically for partially vitrified samples, as it can be seen for $Nd_{30}Fe_{60}Al_{10}$ melt-spun ribbon, 25 μm. In comparison with the magnetization, the coercive field behaviour is completely different, suggesting that the suitable compositions for Nd–Fe–Al amorphous glassy hard magnets are in the range 30–35 at%Fe, for Al content of 10 at%. The difference in the magnetization at $6.4\,MAm^{-1}$ and the spontaneous magnetization is probably due to the ferromagnetic alignment of ordered Nd and Fe moments in external field, whereas without field Nd moments are oriented randomly and Fe moments are aligned ferromagnetic, in agreement with previous reported results for RE-Fe binary amorphous alloys.[3,23] Nd is a light rare earth with less than half of the $4f$ shell occupied and the orbital contribution L dominant. Therefore the usual negative exchange between the rare earth and transition metal, which aligns the spins in opposite directi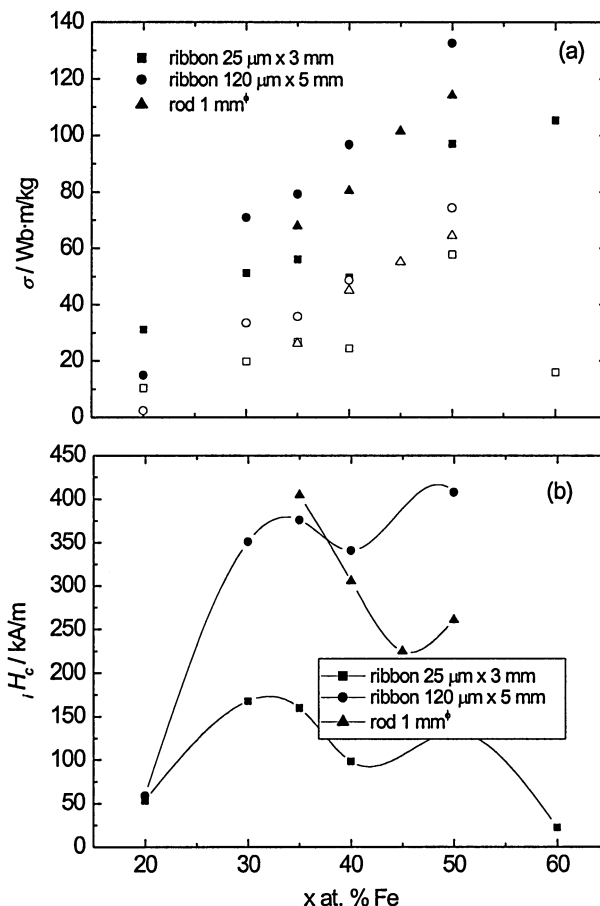ons, will give rise to a ferromagnetic system with Nd and transition metals resulting in the net moments being aligned in the same direction.

The magnetization data from 5 to 285 K were obtained on all the samples in fields up to $7.2\,MAm^{-1}$. Figure 6 shows the magnetization and the coercive field for $Nd_{50}Fe_{40}Al_{10}$ melt-spun amorphous ribbon 25 μm taken between 5 and 280 K and different fields after the sample had been cooled in zero-field from room temperature to 5 K. All the amorphous samples (ribbons and cast rods) exhibit almost the same behavior. As larger as the applied field as smaller the temperature at which the maximum of the coercive field is attained. If the applied field is not enough to rotate the magnetic moments along its direction, the response of the system will be different and consequently the different magnetization behavior observed at low temperatures as a function of applied field.

Figure 7 shows magnetization loops for $Nd_{40}Fe_{50}Al_{10}$ partially vitrified amorphous ribbon 120 μm in thickness taken at different temperatures after the sample had been cooled from 300 to 5 K without field. The loop is clearly shifted upward at 68 K along the magnetization axis, but the reversible magnetization is symmetric about $H = 0$. This behavior is in agreement with the multiphase transitions inferred from the low temperature AC-susceptibility measurements, as it can be seen in Fig. 8. A slight dependence on temperature appears with the increase of the sample thickness and probably is due by the changes of the microstructure depending on the cool-
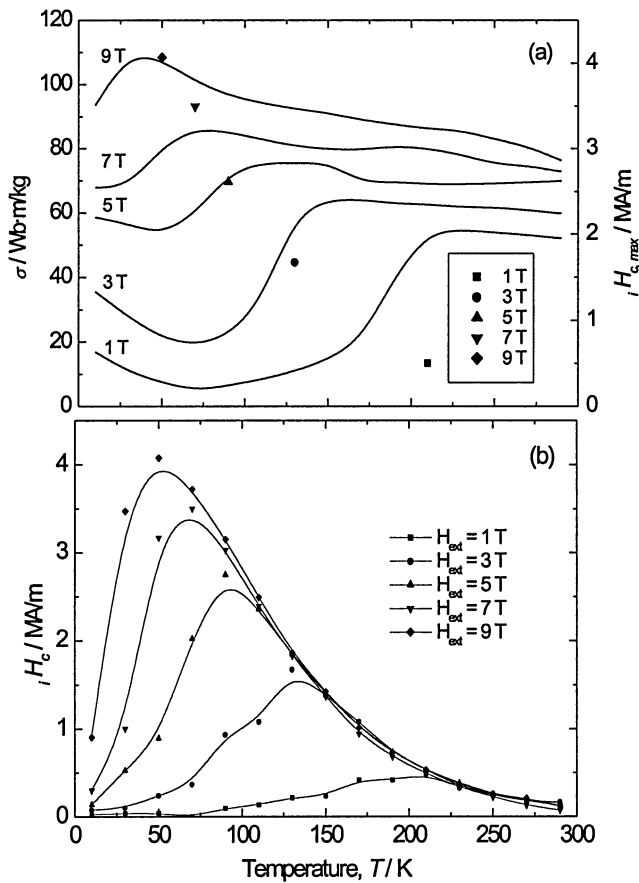
Fig. 6 The magnetization (a) and the coercive field (b) vs. temperature and applied field for $Nd_{50}Fe_{40}Al_{10}$ amorphous melt-spun ribbon 25 μm. The symbols in (a) represents the maximum values of the coercive field and the corresponding temperature.
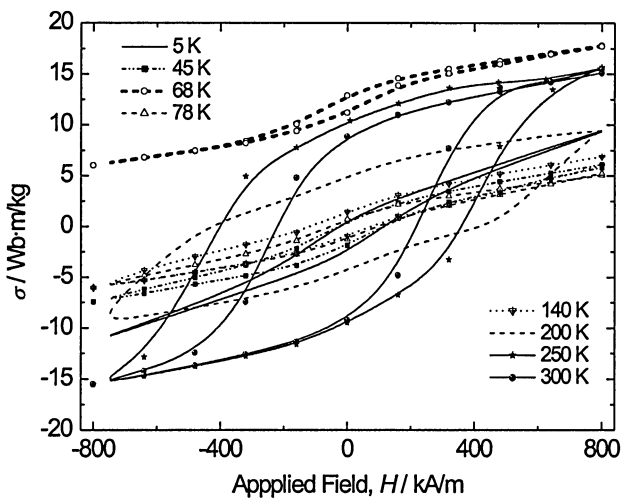

Fig. 7 Zero-field cooled magnetization data $(0.8\,MAm^{-1})$ for $Nd_{40}Fe_{50}Al_{10}$ partially vitrified melt-spun ribbon, 120 μm in thickness, at 5 K; 45 K; 68 K; 78 K; 140 K; 200 K; 250 K and 300 K.

Fig. 8 Real part (χ') and imaginary part (χ'') (insets) of the Ac-susceptibility for $Nd_{50}Fe_{40}Al_{10}$ amorphous melt-spun ribbons and cast rods (a) and $Nd_{40}Fe_{50}Al_{10}$ amorphous melt-spun ribbons 25 μm and cast rod, and partially vitrified melt-spun ribbons 120 μm (b).

ing rate. The imaginary part (χ'') clearly shows differences between the ribbons and bulk amorphous rod being related to the more relaxed amorphous structure existent in bulk samples. The peak in χ' at around 10 K seems to be the Néel temperature of the main Nd-rich antiferromagnetic phase or the freezing temperature below which Nd magnetic moments wil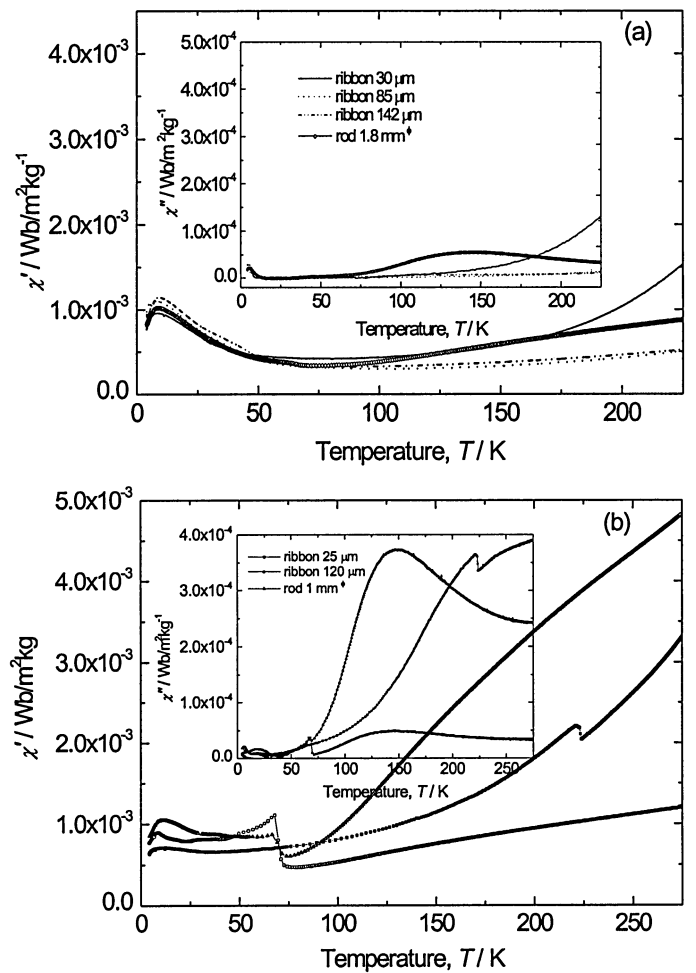l be locked to their local easy axis. It is interesting to note also the existence of one step on the real part around 100 K for amorphous samples, regarding the Fe content), just before χ' starts to increase, which corresponds to the pronounced increase of the coercive field obtained by the DC-magnetic measurements. The real part of AC-susceptibility (χ') for $Nd_{40}Fe_{50}Al_{10}$ partially vitrified thick ribbon 120 μm (Fig. 8(b)) shows a second peak at 68 K, which appears also for the imaginary part (χ''), and is in agreement with the shift upward observed for the hysteresis loop. Above 70 K, the Nd-rich matrix and Fe-based magnetic clusters are magnetically uncoupled and the response of the system is weakly ferromagnetic. The strong increase of the susceptibility with the temperature above 70 K represents the response of the ferromagnetic clusters that cannot be saturated by the available applied fields.

The hysteresis loop at room temperature is the response of the magnetic clusters phase, because the Nd-rich phase is paramagnetic and has no contribution. The annealing at temperatures lower than crystallization temperature ($T_x \cong$ 440°C), as shown in Fig. 9, leaves almost unchanged the magnetic properties, which we suggest is due to the thermal stability of the amorphous alloys. The onset of crystallization leads to the metastable phases' formation, which have larger coercive fields but smaller magnetizations in comparison with
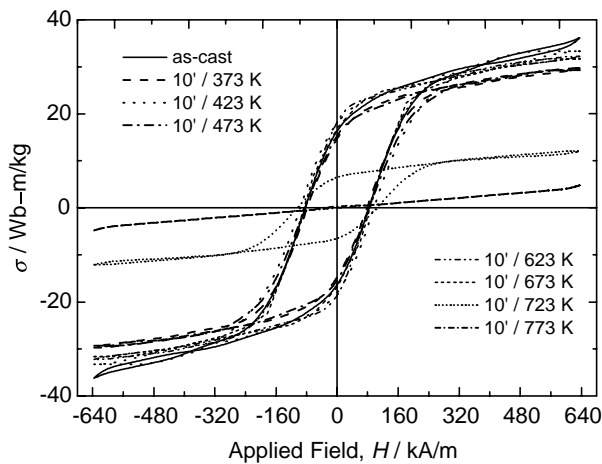
Fig. 9 Hysteresis loops as a function of annealing temperature for $Nd_{50}Fe_{40}Al_{10}$ amorphous ribbon 25 μm thickness.

the amorphous phase. These metastable phases disappear after annealing at 500°C in agreement with XRD and neutron diffraction results, above this temperature the sample being paramagnetic.

3.3 Mössbauer spectroscopy

Figures 10(a) and (b) show Fe^{57} Mössbauer spectra at 300 K on $Nd_{90-x}Fe_xAl_{10}$ ($x = 40$ and 50) amorphous melt-spun ribbons 25 μm. The solid lines are the fits of the data. The Mössbauer data were fitted with two overlapping sextets, one of which is attributed to the Fe-based hard magnetic phase and the other one to dilute Fe in the Nd-rich phase. Figures 10(c) and (d) show the internal field distribution functions deduced from Mössbauer spectra at 300 K. The first two peaks and the last one represent diluted (non-magnetic or paramagnetic) iron contributions to the spectra. The peak at about 22 T represents the magnetic iron contribution to the spectra and its intensity is higher for the amorphous ribbon with 50 at%Fe (c) and is more than 70% of the total intensity.

4. Discussion and conclusions

The structural, magnetic (DC and AC) and Mössbauer spectroscopy studies on $Nd_{90-x}Fe_xAl_{10}$ melt-spun ribbons and cast rods have shown that these bulk amorphous alloys are structurally "glassy" but magnetically "granular". The granular magnetic structure consists in Fe-based nanosized clusters dispersed in the amorphous Nd-rich matrix. Due to their very small dimensions they cannot be evidenced by X-ray diffraction measurements, but their presence is proved by the specific magnetic behavior of these bulk amorphous alloys, especially by the high coercive fields in the as-quenched state and the dependence on the cooling rate. The composition and size of the magnetic clusters as well as the composition of the matrix in which the clusters are embedded are very sensitive to the preparation conditions, mainly the cooling rate and the thermal history of the molten alloy. Fe-based magnetic clusters are coupled between them through the amorphous matrix and the exchange coupling is strongly influenced by the magnitude of the Nd^{3+} single ion local anisotropy. Whereas at low temperatures the anisotropy plays a predominant role

in the macroscopic magnetic response of the system, the increase of the temperature diminishes its effect and the main role is attributed to the ferromagnetic exchange energy. At low temperature, the local anisotropies of the Nd^{3+} ions are very strong and oriented randomly, thus they can "freeze" randomly the magnetic moments of Fe and Nd. The anisotropy axis corresponding to the Fe–Nd pairs are oriented randomly, and a small external field is not enough to align them.

The AC-susceptibility measurements as well as the variation of the coercive field on temperature in the range 4–300 K indicate the magnetic transitions that suggest different local arrangements of the Nd atoms, similar to dhcp (double hexagonal compact) and fcc crystalline phases. The first transition appears around 10 K and seems to be related to the Néel transition temperature of the Nd antiferromagnetic. Another magnetic transition is observed around 70 K and is due to the transition from a completely disordered magnetic phase to a sperrimagnetic non-collinear one. Nd in the dhcp form is antiferromagnetic and exhibits two transition temperatures: the first one at 7.5 K represents the ordering temperature for the cubic B and C sites, and the second one at 19.9 K is the ordering temperature of the hexagonal A sites.[24] But, depending on the nature and the size of the nearest neighbors, Nd could also exist in fcc allotropic form with ferromagnetism below 29 K. Thus, Nd could exist either in dhcp or fcc form in the amorphous matrix of the Nd–Fe-based bulk amorphous alloys. Fe also could be ferromagnetic ($R/r > 1.63$) or antiferromagnetic ($R/r > 1.63$), where R represent the atomic radius and r represent the radius of the incomplete $3d$ inner shell, depending on the coordination number and the nature of the nearest neighbors.[25]

Different magnetic structures can be obtained depending on temperature and the predominant coupling between Fe and Nd atoms. Between 10 and 100 K and for low external fields (< 1 T), Nd-rich matrix and Fe-based magnetic clusters are completely uncoupled, but the exchange coupling within the clusters exist. If from any reason, the coupling between clusters is not possible, the macroscopic response of the system is weakly ferromagnetic. The maximum of the coercive field is attained at the temperature at which the anisotropy energy and the exchange energy have similar values, i.e. the magnetic clusters have the size of the single magnetic domain.[26] Taking into consideration the critical size for the Fe single domain of about 100 nm and the strength of the local anisotropy of the Nd^{3+} ions results that the Fe magnetic moment is not aligned on a direction but forming a cone with an angle of about 30°.[24] Thus, the magnetic structure is non-collinear.

In Nd–Fe-based thin amorphous ribbons, due to their reduced dimensions, high cooling rate (which does not allow the structural relaxation) and thermal effects, the system tends to a superparamagnetic regime at room temperature, and consequently the coercive filed is not very large. It is known that in materials containing single magnetic domains the magnetization is due mainly by the magnetic moments rotations. If the value of the applied field is not large enough, the measured hysteresis loops are minor loops, and the measured magnetization is far from its saturation. This effect is more pronounced in materials in which the magnetic anisotropies play an important role in magnetization processes. Nd–Fe-based bulk amorphous materials with strong local random magnetic
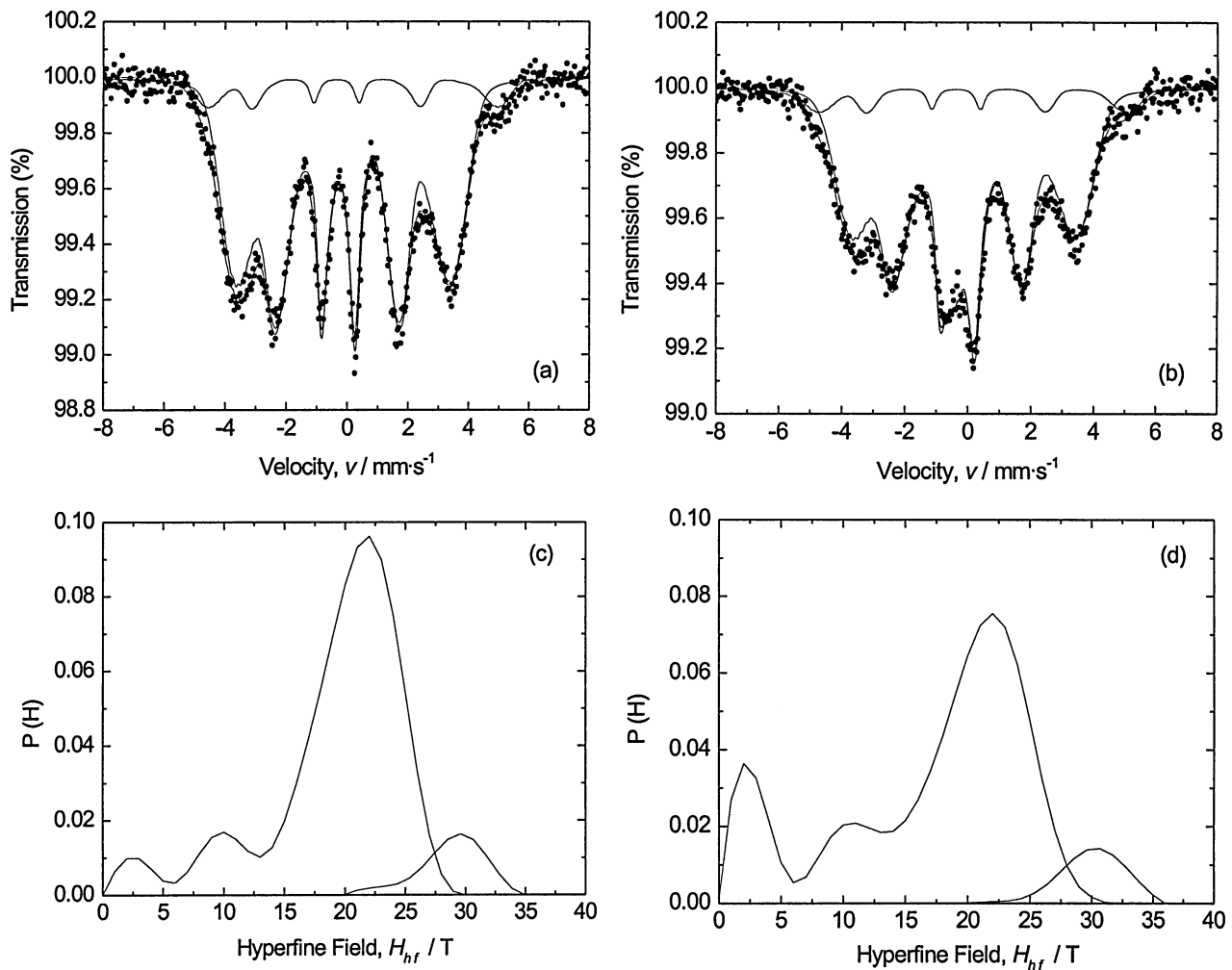
Fig. 10 Fe^{57} Mössbauer spectra (points) and fits (solid curves) for $Nd_{40}Fe_{50}Al_{10}$ (a) and $Nd_{50}Fe_{40}Al_{10}$ (b) amorphous melt-spun ribbons 25 μm in thickness and corresponding $P(H)$ curves at 300 K ((c) and (d)).

anisotropy of the Nd^{3+} ions, which becomes stronger with decreasing the temperature, belong to this class of materials.

The larger the applied field the smaller the temperature at which the coercive field attains its maximum. One observes also that the magnetization exhibits different behavior for applied fields no large enough to align the magnetic moments parallel to its direction, *i.e.* to be large enough to overload the anisotropy energy given by the Nd^{3+} ions anisotropy.

The pair correlation function obtained by Fourier inversion of the diffraction patterns shows first neighbor peaks at 0.254, 0.285 and 0.336 nm. The peak at 0.254 nm is at the position expected for the nearest neighbor Fe atoms in the dense random packing (DRP) model; the other peaks cannot be correlated to combinations of the radii of Nd (0.182 nm), Al (0.143 nm) or Fe (0.127 nm) atoms as predicted by the DRP model. This disagreement could be ascribed to the development of a new type of disordered structure. Thus, one suggests that the structure consists in a dense random packing of nanometer-sized atomic clusters. Consequently, the magnetic structure will consist in non-collinear short-range magnetic ordered regions randomly distributed. In order to prove the existence of these short-range magnetic ordered regions (magnetic clusters) we simulated the topological structure of $Nd_{90-x}Fe_xAl_{10}$ amorphous alloys in the shape of rib-

bons and rods using the reverse Monte Carlo (RMC) method (see Fig. 4). Small Fe-based clusters embedded in a homogeneous Nd-based matrix are observed in the amorphous ribbons and the cast rods, regarding the composition, whereas in the partially vitrified ribbon slabs containing Fe and Al and between them isotropically dispersed Nd and Fe atoms were found out in agreement with the structure proposed for Nd–Fe–Al crystalline compounds.[27]

Despite the considerable progress achieved in recent years concerning the knowledge of the atomic structure of amorphous alloys and concerning the understanding of their basic magnetic properties, there are still many questions related to the microstructure of Nd–Fe-based high coercivity bulk amorphous alloys and its interplay with magnetic properties. The magnetic ground states of Nd–Fe-based cluster amorphous alloys and non-collinear structures existent in these materials are far from being fully characterized. These problems and others make the study of the magnetic properties of bulk amorphous alloys a fascinating field of research.

Although the high-coercivity Nd–Fe-based bulk amorphous alloys are currently more suitable for fundamental research being below those considered necessary for economic viability, they could be used successfully in the future for different applications.

Acknowledgements

REFERENCES

1) J. M. D. Coey: J. Appl. Phys. **49** (1978) 1646–1652.
2) J. J. Croat: J. Magn. Magn. Mater. **24** (1981) 125–131.
3) J. J. Croat: J. Appl. Phys. **52** (1981) 2509–2511.
4) D. Givord, J. P. Noziéres, J. L. Sánchez Llazamares and F. Leccabue: J. Magn. Magn. Mater. **111** (1992) 164.
5) Y. He, C. E. Price, S. J. Poon and G. J. Shiflet: Philos. Mag. Lett. **70** (1994) 371–377.
6) A. Inoue, T. Zhang, W. Zhang and A. Takeuchi: Mater. Trans., JIM **37** (1996) 99–108.
7) H. Chiriac and N. Lupu: J. Magn. Magn. Mater. **196–197** (1999) 235.
8) X. Z. Wang, Y. Li, J. Ding, L. Si and H. Z. Kong: J. Alloys Compd. **290** (1999) 209–215.
9) G. J. Fan, W. Löser, S. Roth, J. Eckert and L. Schultz: Appl. Phys. Lett. **75** (1999) 2984–2986.
10) A. S. O'Connor, L. H. Lewis, R. W. McCallum, K. W. Dennis, M. J. Kramer, D. T. Kim Anh, N. H. Dan, N. H. Luong and N. X. Phuc: Proc. XVI-th Int. Workshop on Rare-Earth Magnets and Their Applications, ed. By H. Kamato, M. Homma, M. Okada (The Japan Inst. Metals, 2000) pp. 475–482.
11) E. Matsubara, T. Zhang and A. Inoue: Sci. Rep. RITU **A43** (1997) 83.
12) H. Chiriac and N. Lupu: J. Non-Cryst. Solids **250–252** (1999) 751–756.
13) R. J. Ortega-Hertogs, A. Inoue and K. V. Rao: Scr. Mater. **44** (2001) 1333–1336.
14) M. J. Kramer, A. S. O'Connor, K. W. Dennis, R. W. McCallum, L. H. Lewis, L. D. Tung and N. P. Duong: IEEE Trans. Magn. **37** (2001) 2497.
15) H. Chiriac, N. Lupu, K. V. Rao and R. E. Vandenberghe: IEEE Trans. Magn. **37** (2001) 2509.
16) P. Gaunt: Can. J. Phys. **65** (1987) 1194–1199.
17) N. Lupu, H. Pattyn and H. Chiriac: unpublished work.
18) A. Wannberg, A. Mellergård, P. Zetterström, R. Delaplane, M. Grönros, L.-E. Karlsson and R. L. McGreevy: J. Neutron Res. **8** (1999) 133–154.
19) http://www.studsvik.uu.se
20) R. L. McGreevy and L. Pustzai: Mol. Simulation H. Chiriac **1** (1988) 359–367.
21) H. A. Alperin, W. R. Gillmor, S. J. Pickart and J. J. Rhyne: J. Appl. Phys. **50** (1979) 1958–1960.
22) N. Lupu, H. Chiriac, A. Takeuchi and A. Inoue: Mat. Res. Soc. Symp. Proc. **674** (2001) U2.7.1–6.
23) R. C. Taylor, T. R. McGuire, J. M. D. Coey and A. Gangulee: J. Appl. Phys. **49** (1978) 2885–2893.
24) K. Moorjani and J. M. D. Coey: *Magnetic Glasses*, (Elsevier, Amsterdam, 1984).
25) R. M. Bozorth: *Ferromagnetism*, (IEEE Press, Piscataway, NJ, 3rd Edition, 1993) pp. 444.
26) B. D. Cullity: *Introduction to Magnetic Materials*, (Addison-Wesley Publishing Company, 1972) pp 385.
27) J. M. Le Breton, J. Teillet, D. Lemarchand and V. De Pauw: J. Alloys Compd. **218** (1995) 31–35.